

Calibration of Computer Models with Heteroscedastic Errors and Application to Plant Relative Growth Rates

Chih-Li Sung^{a1}, Beau David Barber^b, Berkley J. Walker^{c,d}

^aDepartment of Statistics and Probability, Michigan State University

^bDepartment of Agricultural and Biological Engineering, University of Illinois at
Urbana-Champaign

^cMSU-DOE Plant Research Laboratory, Michigan State University

^dDepartment of Plant Biology, Michigan State University

Abstract

Computer models are commonly used to represent a wide range of real systems, but they often involve some unknown parameters. Estimating the parameters by collecting physical data becomes essential in many scientific fields, ranging from engineering to biology. However, most of the existing methods are developed under a homoscedastic error assumption. Motivated by an experiment of plant relative growth rates where replicates are available, we propose a new calibration method for the physical data with heteroscedastic measurement errors. Numerical examples demonstrate that the proposed method not only yields accurate parameter estimation, but it also provides accurate predictions for physical data when the measurement errors are heteroscedastic. We compare this new method to the standard approach used to interpret growth data and give additional examples of how this approach can be used to produce more statistically robust conclusions from computer models of biology and biochemistry in general. We additionally outline how the approach can be used to determine optimal sampling locations.

¹Corresponding author.

Keywords: Replication, Plant Biology, Input-dependent noise, Gaussian process, Uncertainty quantification

1 Introduction

Computer models, which use mathematical representations to simulate real systems, have been widely adopted to understand a real-world feature, phenomenon or event. The applications of computer models range from economics to the physical and biological sciences. For instance, high-fidelity computer simulations are conducted in Mak et al. (2018); Yeh et al. (2018); Wang et al. (2018) to study turbulent flows in a swirl injector, which are used in a wide variety of engineering applications such as the design of contemporary liquid rocket engines. A computer model often contains some unknown parameters that represent certain inherent attributes of the underlying systems but cannot be directly controlled or measurable in its physical experiment, which are called *calibration parameters* in the literature (Santner et al., 2018). When its physical experiment is available, these parameters are used to *calibrate* the computer model such that the model simulations agree with characteristics observed in the physical experiment. This process is called *calibration*, and it is of great importance for computer modelers because it not only improves the model prediction, but the estimated value of the calibration parameters also provides some scientific insight which can help modelers better understand the system. For example, the parameters in the cell adhesion study of Sung et al. (2019) include kinetic rates and their estimated values provide the information of molecular interactions in the biological system. An improved understanding of a biological system is also vital towards efforts to re-engineer improvements to the system of interest.

This paper is motivated by the preponderance of computer models used to interpret biological data, and the inherent limitations to using biological data for this purpose. For example, the underlying biochemistry facilitating carbon fixation by plants can be determined by calibrating a computer model with rates of photosynthesis measured as a

function of light intensity or carbon dioxide concentration (von Caemmerer, 2000; Sharkey et al., 2007; von Caemmerer, 2013). Computer models are also used to quantify plant metabolic fluxes (Ma et al., 2014). Additionally, computer models can help filter large data-sets generated from inherently noisy high-throughput imaging platforms (Xu et al., 2015). We focus here on applications related to plant biology and biochemistry, but this only reflects our direct experience and computer models are used widely in other biological and biochemical systems. Oftentimes gathering and interpreting data from plant science experiments face the same challenges when used in calibration approaches: (1) models are imperfect due to simplifications or incomplete understanding of the system, (2) data contain heteroscedastic variance due to limitations in measurement approaches and variability in plant development and (3) sampling is expensive experimentally and limited by the number of plants that can be grown. For these reasons, plant biology is in need of new approaches to calibrate computer models in statistically robust ways.

Although there has been much work on calibration problems in the statistics literature (e.g., Kennedy and O’Hagan (2001); Tuo and Wu (2015)), these methods are not suitable to our study, because they are developed under a *homoscedastic* assumption, that is, measurement error variances are assumed to be identical over input spaces. In addition, replicates are often available in the plant science experiments, but little attention has been paid to the computational efficiency when replications are conducted in physical experiments. Inspired by Binois et al. (2018), we show that replications have the potential for computational savings for likelihood-based calibration methods through pre-averaging of repeated observations.

In this paper, we propose a new calibration framework for the physical data with heteroscedastic errors, where a heteroscedastic model is introduced which enjoys computational efficiency of inference and prediction under replication. The remainder of this paper is

organized as follows. In Section 2, background of the motivated application, plant relative growth rates, is described. In section 3, a heteroscedastic model for this problem is introduced, and an estimation procedure for the calibration parameters and the hyperparameters in the model is developed. Synthetic examples are illustrated in Section 4. The proposed framework is applied to the case study of plant relative growth rates in Section 5. Concluding remarks are given in Section 6. Estimation details and theoretical proof are provided in Supplementary Materials.

2 Background

We first describe the physical experiment for plant growth rates, and then outline the computer model used to investigate the relative growth rate of plants.

2.1 Plant Growth Experiment

In this experiment, the growth of three groups of plants grown under two different carbon dioxide concentrations was analyzed over a three-week period. The plant species was *Arabidopsis thaliana*, a common experimental plant that is easily manipulated genetically and grows along a flat plane, making growth analysis by overhead imaging of chlorophyll fluorescence possible (Figure 1). Chlorophyll fluorescence is a powerful biophysical signature that arises from photosynthetically active tissue and is an easy signature indicating healthy and growing plant area (Murchie and Lawson, 2013).

In the experiments presented herein, overhead images of *Arabidopsis thaliana* were obtained with a Fluor-Imager Fluorometer (Photon Systems Instruments, Czech Republic) to calculate the overall plant area for a given day as a measure of growth. The *Arabidopsis thaliana* plants were taken from their respective growth chambers and placed in a dark

room for 15 minutes before being moved into the enclosed Fluor-Imager for imaging to minimize light exposure. This process of *dark adaptation* helps emphasize the fluorescence signature of plants by removing actinic lighting for a period of time to reach a steady-state of fluorescence emission (Murchie and Lawson, 2013). The Fluor-Imager illuminates the target plant with actinic light for a brief moment to cause fluorescence emissions to spike such that they can be measured for a short period of time in the post-illumination period.

The three groups of plants differed by the presence or absence of certain genes involved in photorespiration, a plant metabolic process important for processing the consequences of biochemically-fixed oxygen when the atmospheric ratio of CO_2/O_2 is too low (Foyer et al., 2009; Maurino and Peterhansel, 2010; Walker et al., 2016b). When a plant is less able to process fixed oxygen through photorespiration, its growth is slowed or the plant may die entirely. The different plant groups tested lacked distinct steps involved in photorespiration, either a critical enzymatic interconversion step (*glyk*) (Boldt et al., 2005), or a transporter (*plgg*) (Pick et al., 2013) which can be circumvented via other transport mechanisms (Walker et al., 2016a; South et al., 2017). These groups were compared to wild type plants (WT), which have a fully functioning photorespiratory pathway. Under ambient CO_2 concentrations, the CO_2/O_2 is low enough to drive high rates of photorespiration while elevated CO_2 can raise the CO_2/O_2 concentration high enough to minimize rates of photorespiration. We would expect the more severely compromised *glyk* to have a slower growth rate than both *plgg* and WT under ambient CO_2 , and that the growth rate would increase under elevated CO_2 .

Plant growth was quantified by imaging the photosynthetically active areas of the tissues using a camera system that measured fluorescence emitted from photosynthetically active tissues (Murchie and Lawson, 2013). Total projected area of the plants was determined using the image processing software ImageJ (Schneider et al., 2012) to determine the change in

area over the three week period. To account for technical and biological variation, multiple replicates were conducted in this experiment.



Figure 1: *Arabidopsis thaliana*, a common plant used in plant biology research.

2.2 Computer Model

In this study we choose to focus on the relatively simple, yet mechanistically accurate, computer model used to calculate the relative growth rate of plants (Blackman, 1919; Hunt, 1982a,b). This model represents plant biomass as a function of days (x) and a constant relative growth rate (θ) according to:

$$f(x, \theta) = \exp(\theta x). \quad (1)$$

By expressing growth rates as this exponential function, this approach minimizes differences in total plant growth that are attributed to more vigorous early growth similar to how it can

resolve interest rates from initial deposits in compounding bank accounts (Blackman, 1919). In the past, this approach required the destructive harvesting of plants for the measurement of dry weight, but recent advances in image analysis have automated the process for plant species that grow flat against the ground by expressing growth on an area basis (Leister et al., 1999). This approach has the added benefit of tracking growth of a single individual and eliminates the complications of having to consider the pitfalls of calibrating means of different individual plants (Evans and Poorter, 2001; Hoffmann and Poorter, 2002).

3 Heteroscedastic Modeling for Calibration Problems under Replication

Suppose that N observations are collected from the physical experiments, denoted by y_1, \dots, y_N , and their corresponding inputs are x_1, \dots, x_N , where $x_i \in \chi \subseteq \mathbb{R}^d$. In the case of replication, we further denote $\bar{x}_i, i = 1, \dots, n$ as the n unique input locations, where $n < N$, and $y_i^{(j)}$ as the j -th output out of $a_i \geq 1$ replicates at the unique location \bar{x}_i , and denote its sample mean, $\sum_{j=1}^{a_i} y_i^{(j)} / a_i$, as \bar{y}_i . Furthermore, denote $f(x, \theta)$ as the computer model which is a deterministic function of the input $x \in \chi \subseteq \mathbb{R}^d$ and the calibration parameter $\theta \in \Theta \subseteq \mathbb{R}^q$. The computer model $f(x, \theta)$ is assumed to be known or cheap to evaluate at any input. The generalization to expensive computer models will be discussed in Section 3.3. Then, the calibration problem with heteroscedastic errors can be modeled as follows,

$$y(x_i) = \zeta(x_i) + \epsilon_i, \quad i = 1, \dots, N, \quad (2)$$

where

$$\zeta(x_i) = f(x_i, \theta) + b_\theta(x_i), \quad (3)$$

and ϵ_i is the measurement or some stochastic error from the real system and independently and identically follows an normal distribution with zero mean and variance $\mathbb{V}[\epsilon_i] = r(x_i)$. The function $\zeta(\cdot)$ is the *true process* of the real system, and the function $b_\theta(\cdot)$ in (3) is the *discrepancy* (or *bias*) between the true process and the computer model. The inclusion of the discrepancy term in the model is necessary because computer models are often considered *inexact* or *imperfect*, meaning that even with an optimal calibration parameter, the computer model does not perfectly match the true process, which is referred as model uncertainty in the literature (Kennedy and O’Hagan, 2001). Note that the dependance of $b_\theta(\cdot)$ on θ is often suppressed in the literature, but it is included here for clarity.

The inexact computer models were first discussed by Kennedy and O’Hagan (2001) which model the model discrepancy as a Gaussian process (GP) model, and this method has been widely used in many applications (e.g., Higdon et al. (2004, 2008); Wang et al. (2009); Han et al. (2009)). Following the idea of Kennedy and O’Hagan (2001), we assume that the distribution of $b_\theta(\cdot)$ is represented by a GP with zero mean and a positive-definite covariance function c , so that $b_\theta(x_1), \dots, b_\theta(x_N)$ is a multivariate normal distribution with zero mean and covariance matrix $(c(x_i, x_j))_{1 \leq i \leq j \leq N}$. A scale $\nu > 0$ is commonly separated from a kernel function, $c(x_i, x_j) = \nu k(x_i, x_j; \boldsymbol{\varphi})$, where $\boldsymbol{\varphi}$ are hyperparameters of the kernel. The dependency of $\boldsymbol{\varphi}$ will be suppressed in the rest of the paper for notational simplicity. Typical choices of the kernel function are Gaussian or Matérn kernels which are independent of θ . However, recent studies (e.g., Gramacy et al. (2015); Tuo and Wu (2015, 2016); Plumlee (2017)) indicate that these choices of kernel functions may lead to unreasonable calibration parameter estimation due to *unidentifiability* of the calibration parameters. Therefore, in this paper, we consider an *orthogonal kernel function* (Plumlee, 2017) to avoid the identifiability issue, which will be introduced in Section 3.2.

Thus, given the noise function $r(x)$, the observations $\mathbf{Y}_N = (y_1, \dots, y_N)$ follow a

multivariate normal distribution,

$$\mathbf{Y}_N \sim \mathcal{N}(\mathbf{f}(\theta), \nu(\mathbf{K}_N + \mathbf{\Lambda}_N)),$$

where $\mathbf{f}(\theta) = (f(x_1, \theta), \dots, f(x_N, \theta))^T$, \mathbf{K}_N is an $N \times N$ matrix with ij elements $k(x_i, x_j)$, and $\mathbf{\Lambda}_N$ is a $N \times N$ diagonal matrix with diagonal elements $\lambda_1, \dots, \lambda_N$, where $\lambda_i = r(x_i)/\nu$. Based on the properties of conditional multivariate normal distributions, the predictive distribution of $y(x)$ at a new input setting x , $y(x)|\mathbf{Y}_N$, is a normal distribution, $\mathcal{N}(\mu(x), \sigma^2(x))$, where

$$\mu(x) = f(x, \theta) + \mathbf{k}(x)^T (\mathbf{K}_N + \mathbf{\Lambda}_N)^{-1} (\mathbf{Y}_N - \mathbf{f}(\theta))$$

and

$$\sigma^2(x) = \nu k(x, x) + r(x) - \nu \mathbf{k}(x)^T (\mathbf{K}_N + \mathbf{\Lambda}_N)^{-1} \mathbf{k}(x), \quad (4)$$

where $\mathbf{k}(x) = (k(x, x_1), \dots, k(x, x_N))^T$.

The main difference of the model from the ones in the literature lies in the the heteroscedastic error ϵ_i whose variance $r(x)$ is non-constant, while typical homoscedastic cases consider a constant variance, $r(x_i) = \tau^2$. This assumption makes the calibration more challenging, because the noise function $r(x)$ is unknown and needs to be estimated. A straightforward and sensible estimate is the sample variance of the replicates at each unique location, that is, $\hat{r}(\bar{x}_i) = \sum_{j=1}^{a_i} (y_i^{(j)} - \bar{y}_i)^2 / (a_i - 1)$. The estimate was used in Ankenman et al. (2010) for fitting a stochastic GP and also commonly used in the metabolic engineering literature for calibrating the parameter θ . For instance, Antoniewicz et al. (2006) estimates the calibration parameters θ (or metabolic flux in their context) by minimizing the weighted least-squares,

$$\hat{\theta}_{\text{WLS}} = \underset{\theta \in \Theta}{\operatorname{argmin}} \sum_{i=1}^n \frac{(\bar{y}_i - f(\bar{x}_i, \theta))^2}{\hat{r}(\bar{x}_i)}. \quad (5)$$

This estimate $\hat{r}(\bar{x}_i)$, however, often requires a minimal number of replicates. For example, Ankenman et al. (2010) recommends $a_i \geq 10$ replicates for fitting a stochastic GP while Wang and Haaland (2019) recommends $a_i \geq 5$. This is impractical in many applications because physical data from a real system is often time-consuming or too costly to collect. In addition, the predictive variance (4) still requires the value of $r(x)$ at the new input setting x but physical data at this input setting is not directly available for estimation. To this end, here we employ the latent log-variance GP proposed by Binois et al. (2018) to model the noise function $r(\cdot)$, which does not require a minimal number of the replicates and is computationally efficient under replications. This model will be briefly reviewed in the next subsection.

3.1 Latent Variable Process for Modeling $r(\cdot)$

Since $r(\cdot) = \nu\lambda(\cdot)$, we instead model $\lambda(\cdot)$ and $r(\cdot)$ can then be obtained by multiplying the scale ν . Denote $\mathbf{\Lambda}_n = (\lambda(\bar{x}_1), \dots, \lambda(\bar{x}_n))$ and $\mathbf{A}_n = \text{diag}(a_1, \dots, a_n)$. Similar to Goldberg et al. (1998) which suggests a GP prior for $\log \lambda(\cdot)$, Binois et al. (2018) models $\log \lambda_1, \dots, \log \lambda_n$ as derived quantities obtained via the predictive mean of a regularizing GP on new latent variables, $\delta_1, \dots, \delta_n$:

$$\log \mathbf{\Lambda}_n = \mathbf{K}_{(g)} (\mathbf{K}_{(g)} + g\mathbf{A}^{-1})^{-1} \mathbf{\Delta}_n,$$

where $\mathbf{\Delta}_n = \text{diag}(\delta_1, \dots, \delta_n)$, $\mathbf{K}_{(g)} = (k_{(g)}(\bar{x}_i, \bar{x}_j))_{1 \leq i, j \leq n}$ is the kernel matrix whose nugget is g , and $\mathbf{\Delta}_n \sim \mathcal{N}(0, \nu_{(g)}(\mathbf{K}_{(g)} + g\mathbf{A}^{-1}))$. $k_{(g)}$ is a kernel function of this noise process, and it contains some hyperparameters which are denoted by ϕ . Typical kernels such as Gaussian or Matérn kernels can be used here. The latent variable $\mathbf{\Delta}_n$ are unknown and treated as additional parameters, which will be estimated in Section 3.4 along with ϕ and

nugget g . The predictive value of $\log \lambda(x)$ at a new input x can then be obtained by $\log \lambda(x) = \mathbf{k}_{(g)}(x)^T (\mathbf{K}_{(g)} + g\mathbf{A}^{-1})^{-1} \Delta_n$, where $\mathbf{k}_{(g)}(x) = (k_{(g)}(x, \bar{x}_1), \dots, k_{(g)}(x, \bar{x}_N))^T$. We refer more details of the latent log-variance GP to Binois et al. (2018).

3.2 Orthogonal Gaussian Process for Modeling $b_\theta(\cdot)$

Although the GP modeling of Kennedy and O’Hagan (2001) for $b_\theta(\cdot)$ has been widely used, recent studies have raised concerns about its identifiability issue of the calibration parameters (Loeppky et al., 2006; Bayarri et al., 2007a,b; Han et al., 2009; Gramacy et al., 2015; Tuo and Wu, 2015, 2016; Plumlee, 2017; Wong et al., 2017). In particular, Tuo and Wu (2016) defines the true parameter as the L_2 distance projection of θ ,

$$\theta^* = \arg \min_{\theta \in \Theta} \|\zeta(\cdot) - f(\cdot, \theta)\|_{L_2(\chi)}, \quad (6)$$

where $\|g\|_{L_2(\chi)} = \int_\chi g(x)dx$, and they show that the estimator of Kennedy and O’Hagan (2001) is asymptotically inconsistent. Plumlee (2017) further points out that the GP modeling of the bias $b_\theta(\cdot)$ should depend on θ , but the one in Kennedy and O’Hagan (2001) does not. Therefore, Plumlee (2017) considers the definition of (6), and provides an alternative GP modeling by *orthogonalizing* the model bias to avoid mixing the GP and the definition of the parameter.

Suppose that $k_0(\cdot, \cdot)$ is any valid kernel function on $\chi \times \chi$ and is independent of θ , such as Gaussian or Matérn kernels. Under the definition of (6), Plumlee (2017) suggests a GP on the bias with the *orthogonal kernel function*,

$$k(x_i, x_j) = k_0(x_i, x_j) - h_\theta(x_i)^T H_\theta^{-1} h_\theta(x_j), \quad (7)$$

where

$$h_\theta(x) = \int_\chi \frac{\partial}{\partial \theta} f(\xi, \theta) k_0(x, \xi) d\xi$$

and

$$H_\theta = \int_\chi \int_\chi \frac{\partial}{\partial \theta} f(\xi_1, \theta) \left(\frac{\partial}{\partial \theta} f(\xi_2, \theta) \right)^T k_0(\xi_1, \xi_2) d\xi_1 d\xi_2.$$

As a matter of fact, the method can be simply generalized to other definitions of the true calibration parameters, such as the L_2 projection with a weighting measure (Plumlee, 2017). Note that the orthogonal kernel function $k(\cdot, \cdot)$ is dependent of θ but here it is suppressed for notational simplicity.

In practice, there are two major difficulties to evaluate $k(\cdot, \cdot)$. The first is the integrals in h_θ and H_θ which are often difficult to solve. This can be addressed by using the stochastic average approximation, such as Monte Carlo integration (Caffisch, 1998). For example, one can uniformly draw m samples, ξ_1, \dots, ξ_m , from χ , and then approximate $h_\theta(x)$ by

$$h_\theta(x) \approx \sum_{i=1}^m \frac{\partial}{\partial \theta} f(\xi_i, \theta) k_0(x, \xi_i).$$

Second, $k(\cdot, \cdot)$ requires the values of the computer model, $f(x, \theta)$, and its gradient, $\partial f(x, \theta) / \partial \theta$, at any input pair $(x, \theta) \in \chi \times \Theta$, but they are not generally obtainable, because computer simulations can be computationally demanding (e.g., the high-fidelity simulation in Mak et al. (2018)). A common approach is to run a computer experiment with various inputs and build an cheaper *emulator* for the actual computer simulations, for which GP modeling is often used (Sacks et al., 1989; Santner et al., 2018). Thus, the predictive distribution of the emulator can be taken as a fixed probabilistic definition of $f(\cdot, \cdot)$, and hence the definition of orthogonal kernel function is modified accordingly. We refer more details to Plumlee (2017).

3.3 Parameter Estimation

In this section, we develop an estimation procedure for the model parameters along the lines described in Binois et al. (2018), which developed fast GP inference and prediction under replication by making use of Woodbury identity to reduce computational complexity. The model parameters include the calibration parameters θ , the hyperparameters of the two GPs, $\boldsymbol{\varphi}, \boldsymbol{\phi}, g$, and the latent variables $\delta_1, \dots, \delta_n$. Conditional on the parameters $\boldsymbol{\omega} \equiv (\theta, \boldsymbol{\varphi}, \boldsymbol{\phi}, g, \delta_1, \dots, \delta_n)$, the scales ν and $\nu_{(g)}$ both have plug-in MLEs: $\hat{\nu} = N^{-1} (\mathbf{Y}_N - \mathbf{f}(\theta))^T (\mathbf{K}_N + \boldsymbol{\Lambda}_N)^{-1} (\mathbf{Y}_N - \mathbf{f}(\theta))$ and $\hat{\nu}_{(g)} = n^{-1} \boldsymbol{\Delta}_n^T (\mathbf{K}_{(g)} + g\mathbf{A}_n^{-1})^{-1} \boldsymbol{\Delta}_n$. The log-likelihood conditional on $\hat{\nu}$ and $\hat{\nu}_{(g)}$ is then

$$\begin{aligned} \log L = & -\frac{N}{2} \log 2\pi - \frac{N}{2} \log \hat{\nu} - \frac{1}{2} \log |\mathbf{K}_N + \boldsymbol{\Lambda}_N| - \frac{N}{2} \\ & - \frac{n}{2} \log 2\pi - \frac{n}{2} \log \hat{\nu}_{(g)} - \frac{1}{2} \log |\mathbf{K}_{(g)} + g\mathbf{A}_n^{-1}| - \frac{n}{2}, \end{aligned} \quad (8)$$

where the top line above is the mean-field component and the bottom line is the variance-field component. The computation complexity of the inverse and determinant of $\mathbf{K}_N + \boldsymbol{\Lambda}_N$ can be reduced by using the Woodbury identity (Harville, 1998). Particularly, denote $\mathbf{K}_n = (k(\bar{x}_i, \bar{x}_j))_{1 \leq i, j \leq n}$, $\bar{\mathbf{Y}}_n = (y(\bar{x}_1), \dots, y(\bar{x}_n))$, and $\bar{\mathbf{f}}(\theta) = (f(\bar{x}_1, \theta), \dots, f(\bar{x}_n, \theta))$, then we have

$$\begin{aligned} (\mathbf{Y}_N - \mathbf{f}(\theta))^T (\mathbf{K}_N + \boldsymbol{\Lambda}_N)^{-1} (\mathbf{Y}_N - \mathbf{f}(\theta)) &= (\mathbf{Y}_N - \mathbf{f}(\theta))^T \boldsymbol{\Lambda}_N^{-1} (\mathbf{Y}_N - \mathbf{f}(\theta)) \\ &- (\bar{\mathbf{Y}}_n - \bar{\mathbf{f}}(\theta))^T \mathbf{A}_n \boldsymbol{\Lambda}_n^{-1} (\bar{\mathbf{Y}}_n - \bar{\mathbf{f}}(\theta)) + (\bar{\mathbf{Y}}_n - \bar{\mathbf{f}}(\theta))^T (\mathbf{K}_n + \mathbf{A}_n^{-1} \boldsymbol{\Lambda}_n)^{-1} (\bar{\mathbf{Y}}_n - \bar{\mathbf{f}}(\theta)) \end{aligned} \quad (9)$$

for computing $\hat{\nu}$, and

$$\log |\mathbf{K}_N + \mathbf{\Lambda}_N| = \log |\mathbf{K}_n + \mathbf{A}_n^{-1} \mathbf{\Lambda}_n| + \sum_{i=1}^n [(a_i - 1) \log \lambda_i + \log a_i]. \quad (10)$$

This reduces the computational complexity of the log-likelihood from $O(N^3)$ to $O(n^3 + N)$. The parameters can then be efficiently estimated by maximizing the log-likelihood via an optimization algorithm. Following the idea of Binois et al. (2018), we use a Newton-like optimization method since the gradient of the log-likelihood is available in a closed form, which is provided in Supplementary Material S1. The R (R Core Team, 2018) code is available in the supplementary materials for implementation, which is via modifications to the source code of R package `hetGP` (Binois and Gramacy, 2019). In particular, the optimization is done by the `optim` library with `method="L-BFGS-B"`, which performs a quasi-Newton optimization method of Byrd et al. (1995). When the gradient, $\partial f(x, \theta)/\partial \theta$, in the orthogonal function of (7) is not available, the function `gradient` in the R package `rootSolve` (Soetaert, 2009) is used to approximate the gradient.

Sweeting (1980) has given a general result of maximum likelihood estimators concerning their weakly consistency and uniform asymptotic normality. Therefore, based on the results of Sweeting (1980) and Mardia and Marshall (1984), we can show that, under some regularity conditions that are given in Supplementary Material S2, the maximum likelihood estimators of $\boldsymbol{\omega}$, which are denoted by $\hat{\boldsymbol{\omega}}_N$, are asymptotically normally distributed as N is sufficiently large.

Theorem 3.1. *Under the regularity conditions given in Supplementary Material S2, the maximum likelihood estimators, $\hat{\boldsymbol{\omega}}$, are weakly consistent and asymptotically normal as $N \rightarrow \infty$; that is,*

$$\hat{\boldsymbol{\omega}}_N \xrightarrow{d} \mathcal{N}(\boldsymbol{\omega}, \mathbf{B}_N^{-1}),$$

where $\mathbf{B}_N = -\mathbb{E}[\partial^2 \log L / \partial \boldsymbol{\omega} \partial \boldsymbol{\omega}^T]$.

This result can be used to construct the confidence intervals for the parameters, especially for the calibration parameter θ , which is the main interest of the study.

4 Illustrative Example

In this section, numerical experiments are conducted to demonstrate the calibration performance of the proposed method. We consider two synthetic data, which are adapted from the examples of Plumlee (2017) and Tuo and Wu (2015).

In the implementation of the proposed method, Matérn kernels are chosen for $k_{(g)}$, which have the form

$$k_{(g)}(x, y) = \left(1 + \frac{\sqrt{5}}{\phi} \|x - y\| + \frac{5}{3\phi^2} \|x - y\|^2 \right) \exp \left(-\frac{\sqrt{5}}{\phi} \|x - y\| \right).$$

Matérn kernels with hyperparameter $\boldsymbol{\varphi}$ are chosen for k_0 in (7) to derive the orthogonal kernel k .

4.1 Example 1

We consider an example modified from Plumlee (2017). Assume that the input $x \in [0, 1]$ and the true process is $\zeta(x) = 4x^2 + x \sin(5x)$, and the observations are given by $y_i = \zeta(x_i) + \epsilon_i$, where ϵ_i is independently normally distribution with zero mean and the variance $r(x_i) = 0.002(\exp(5x) + 0.2)$. Suppose that the computer output is given by the function $f(x, \theta) = \theta x$, where $\theta \in [0, 10]$. By minimizing the L_2 distance as in (6), we have the true parameter $\theta^* \approx 2.5725$. This computer model is *imperfect* because even with the optimal setting θ^* , there still exists discrepancy between $f(\cdot, \theta^*)$ and $\zeta(\cdot)$.

In this numerical study, eight unique input locations are selected with equal space in $[0, 1]$, and 5 replicates are generated at each unique location, that is, $a_1 = \dots = a_8 = 5$. Figure 2 demonstrates the simulated data with $a = 5$ replicates at each location, in which three different methods are performed, which are: (left) the weighted least-squares of (5); (middle) the homoscedastic modeling of Kennedy and O’Hagan (2001); (right) our proposed method. The calibration parameter estimates are 2.4833, 2.7974, and 2.6115, respectively, and their corresponding L_2 distances are 0.1413, 0.1851, and 0.1335. In this example, our proposed method provides a more accurate parameter estimate (the true parameter is $\theta^* \approx 2.5725$), which also can be seen from the upper panels, where the computer model with the estimate is closer to the true process than other two methods in the sense of L_2 distances. Inaccurate estimation could produce serious erroneous results and confer incorrect interpretation of the parameter, as its estimates are often used for understanding a real system, such as the relative growth rates in our case study. Figure 2 also shows that the weighted least-squares yield inaccurate predictions for physical data, and the homoscedastic modeling of Kennedy and O’Hagan (2001) suggests unreasonably wide prediction intervals due to the constant variance assumption. On the other hand, the proposed method not only provides a more accurate parameter estimate, but it also provides more accurate predictions as well as more reasonable prediction intervals by recovering the variance process.

We conduct the simulation 100 times to examine the performance of our proposed method (labeled **HetOGP**), in comparison with the weighted least-squares (labeled **WLS**), homoscedastic modeling of Kennedy and O’Hagan (2001), with a Matérn kernel (labeled **HomGP**), homoscedastic modeling with an orthogonal kernel (labeled **HomOGP**), and heteroscedastic modeling with a Matérn kernel (labeled **HetGP**). Three main metrics are used for the comparison: (i) estimation bias, $\hat{\theta} - \theta^*$; (ii) root mean squared errors (RMSEs) based on 101 test equal-spaced locations in $[0, 1]$, $(\sum_{i=1}^{101} (\zeta(x_i) - \hat{y}(x_i))^2 / 101)^{1/2}$, where $\hat{y}(x)$

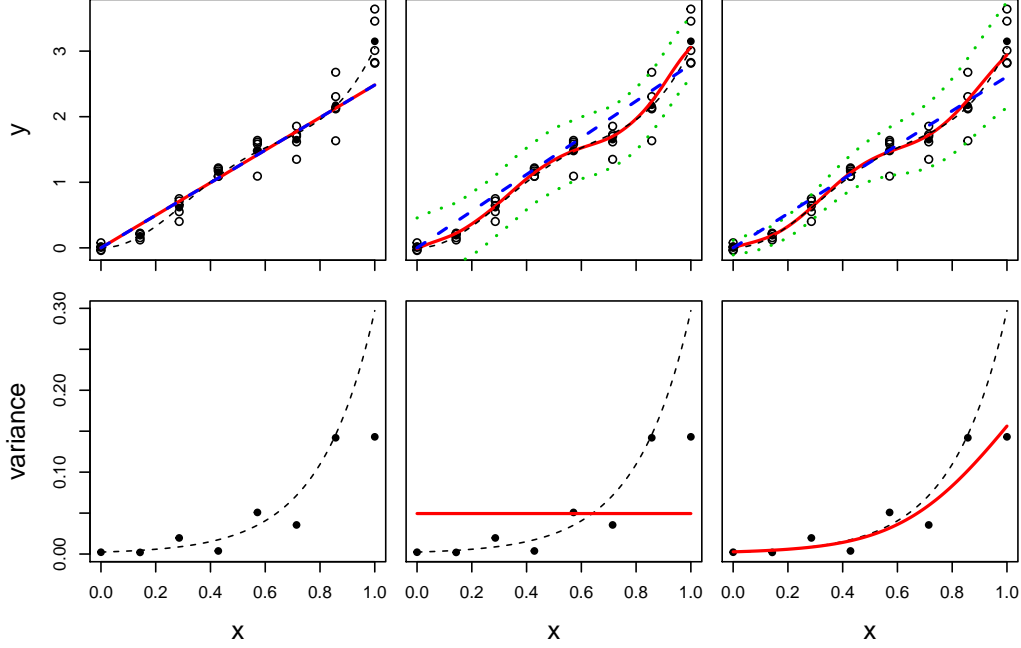


Figure 2: *Illustration of three methods for the first example: (left) weighted least-square; (middle) Kennedy and O'Hagan's approach; (right) the proposed method. Upper panels represent the replicates as open circles with the averaged observation \bar{y}_i in filled circles at each unique input location, the true process as a black dashed line, the computer model $f(\cdot, \hat{\theta})$ as a blue dashed line, and the prediction mean curve as a red solid line, with 95% prediction intervals in green dotted lines. Lower panels represent the sample variance $\hat{r}(\bar{x}_i)$ as black points, the true variance process as a dashed line, and the fitted variance process as a red solid line.*

is the prediction mean for the input x ; (iii) predictive score, which is a scoring rule provided by Equation (27) of Gneiting and Raftery (2007) that combines prediction means and variances. Since the true distribution of y_i is known in the simulation setting, the predictive score has the form as follows,

$$-\frac{1}{100} \sum_{i=1}^{100} \left(\frac{\zeta(x_i) - \hat{y}(x_i)}{\hat{\sigma}^2(x_i)} \right)^2 - \frac{r(x_i)}{\hat{\sigma}^2(x_i)} - \log \hat{\sigma}^2(x_i),$$

where $\hat{\sigma}^2(x)$ is the prediction variance for the input x .

Figure 3 shows the results for the five methods based on the 100 simulations. The predictive score of **WLS** is not available because the prediction variances at unobserved input locations are not available for the weighted least squares. First, from the left panel, it can be seen that our proposed method (**HetOGP**) outperforms the other methods in terms of calibration parameter estimation. Moreover, from the middle and right panels, it shows that although the prediction accuracy is not significantly different except for **WLS**, the prediction scores of heteroscedastic modeling-based methods (**HetGP** and **HetOGP**) are significantly higher than homoscedastic modeling-based methods (**HomGP** and **HomOGP**). The reason is that, as shown in Figure 2, the homoscedastic modeling yields unreasonable wide prediction intervals in this heteroscedastic case. In terms of computational cost, all the methods here are implemented within 3 seconds, on a laptop with 2.6 GHz CPU and 16 GB of RAM. Based on the estimation and prediction results, it suggests that our proposed method is more appropriate for this calibration problem, which provides more accurate parameter estimation along with high prediction accuracy and prediction scores.

4.2 Example 2

We consider another example which is modified from Tuo and Wu (2015). Assume that the input $x \in [0, 2\pi]$ and the true process is $\zeta(x) = \exp(x/10) \sin x$, and the observations are given by $y_i = \zeta(x_i) + \epsilon_i$, where ϵ_i is independently normally distribution with zero mean and the variance $r(x_i) = (0.01 + 0.2(x_i - \pi)^2)^2$. Suppose that the computer output is given by the function $f(x, \theta) = \zeta(x) - \sqrt{\theta^2 - \theta + 1}(\sin \theta x + \cos \theta x)$. It can be seen that there does not exist a real number θ such that $f(\cdot, \theta) = \zeta(\cdot)$, because $\sqrt{\theta^2 - \theta + 1}(\sin \theta x + \cos \theta x)$ is always positive for any θ . Thus, the computer model is also imperfect. By minimizing the L_2 distance as in (6), we have the true parameter $\theta^* \approx -0.1789$.

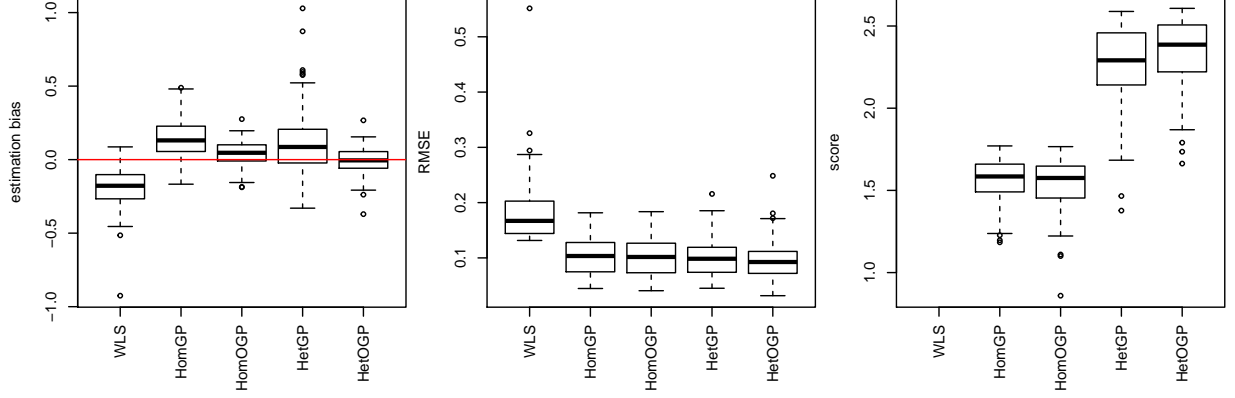


Figure 3: The comparison of estimation and prediction performance for the first example. The left panel represents the estimation bias of the calibration parameter, with the red horizontal line with an intercept of zero. The middle panel shows their root mean squared errors, and the right panel represents their predictive scores.

Similar to the setup in the previous subsection, eight unique input locations are selected with equal space in $[0, 2\pi]$ and 5 replicates are generated at each unique location. Figure 4 shows the simulated data and the performance of the three methods: **WLS** (left), **HomGP** (middle), and **HetOGP** (right). The calibration parameter estimates are -0.2784, 0.2674, and -0.1751, respectively, and their corresponding L_2 distances are 0.7841, 1.1276, and 0.5822. Similarly, our proposed method provides a more accurate parameter estimate in this example (the true parameter is $\theta^* \approx -0.1789$), which also can be seen from the upper panels, where the computer model with the estimate is closer to the true process than other two methods in the sense of L_2 distances. **WLS** performs poorly in terms of parameter estimation and prediction for physical data. **HomGP** suggests a biased parameter estimate and unreasonably wide prediction intervals, even though the prediction mean is accurate in this example. The proposed method (**HetOGP**), as in the previous subsection, not only provides an accurate parameter estimate, but the prediction mean and intervals are also more appropriate.

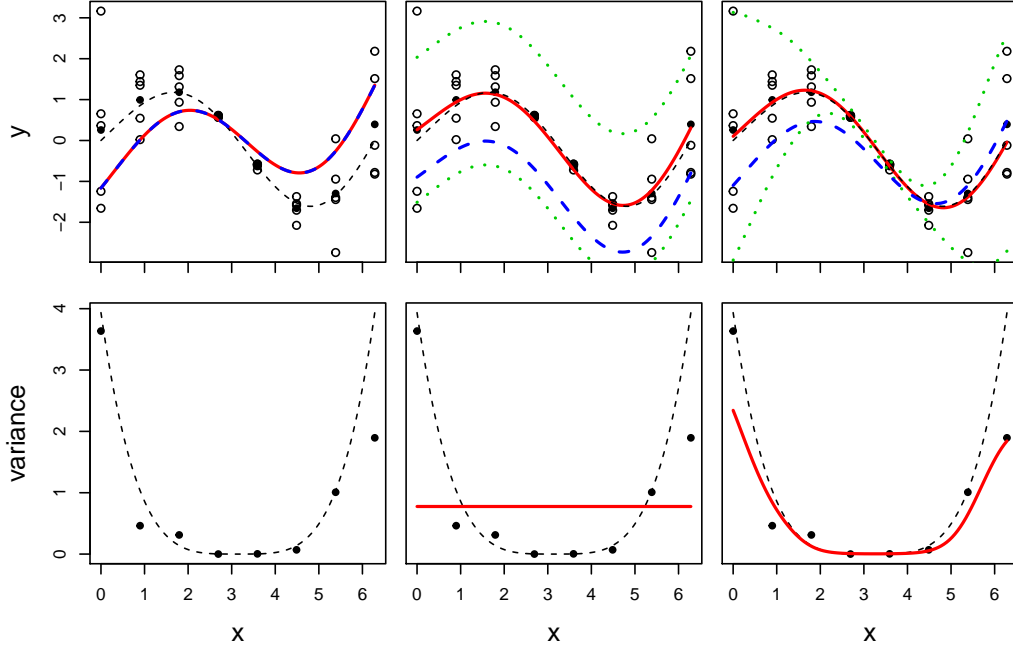


Figure 4: Illustration of three methods for the second example: (left) weighted least-square; (middle) Kennedy and O'Hagan's approach; (right) the proposed method. Upper panels represent the replicates as open circles with the averaged observation \bar{y}_i in filled circles at each unique input location, the true process as a black dashed line, the computer model $f(\cdot, \hat{\theta})$ as a blue dashed line, and the prediction mean curve as a red solid line, with 95% prediction intervals in green dotted lines. Lower panels represent the sample variance $\hat{r}(\bar{x}_i)$ as black points, the true variance process as a dashed line, and the fitted variance process as a red solid line.

Similar to the previous subsection, we conduct the simulations 100 times to compare the proposed method with the other four methods. Figure 5 shows the comparison using the three metrics in the previous subsection. It can be seen that, the estimates of WLS are very biased, which result in poor prediction. HomOGP gives relatively unbiased estimates, but the prediction accuracy and scores perform worse than heteroscedastic modeling. HetGP results in superior prediction accuracy and prediction scores, but the estimates are quite off from the true parameter. As pointed out by Tuo and Wu (2015), GP modeling for

the discrepancy function from an imperfect computer model may lead to unreasonable estimation. This issue also occurs in the heteroscedastic case. On the other hand, our proposed method (HetOGP), which models the discrepancy function using an orthogonal GP, provides more accurate parameter estimation, along with high prediction accuracy and prediction scores.

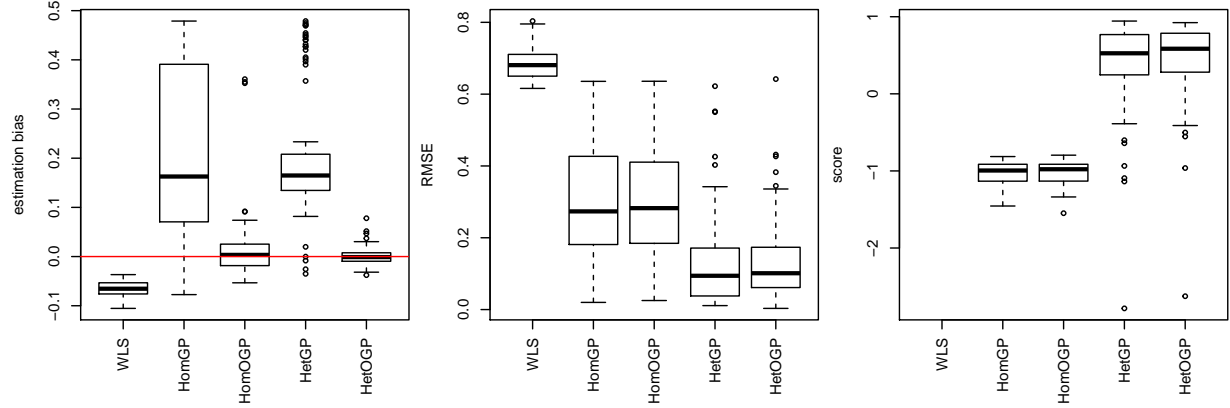


Figure 5: The comparison of estimation and prediction performance for the second example. The left panel represents the estimation bias of the calibration parameter, with the red horizontal line with an intercept of zero. The middle panel shows their root mean squared errors, and the right panel represents their predictive scores.

5 Case Study of Plant Growth Rate

In this section, we leverage the statistical developments to investigate the plant relative growth rates for the plants grown under ambient and high CO_2 concentrations, with three plant groups that were described in Section 2.1: *glyk*, *plgg*, and WT. The experimental data consists of the total projected areas of the plants at 8 unique time points, as the input variable $x \in [0, 20]$, and for each unique time point, three to five replicates are measured.

The computer model is as described in (1), which shares the same input variable x (time) and has a calibration parameter, the relative growth rate, $\theta \in [0, 1]$.

5.1 Calibration Results

The calibration results of the experimental data under ambient and high CO₂ concentrations are presented in Figures 6 and 7, respectively. First, it can be seen that in the experimental data under both ambient and high CO₂ concentrations, the variances tend to increase as the time increases, which indicates that the heteroscedastic modeling is essential for this data. Our approach takes into account the heteroscedasticity and provides the fitted variance process (as the red lines in the middle panels), which in turn gives sensible prediction intervals (as the green dotted lines in the top panels). Moreover, bottom panels present the fitted discrepancy function, $b_{\hat{\theta}}(x)$, with 95% pointwise confidence intervals based on the orthogonal GP modeling in Section 3.2. The discrepancy functions show that the computer model is imperfect as expected, especially for the data under CO₂ ambient concentrations (Figure 6), which may suggest that a quadratic polynomial is needed in the computer model. Future studies of plant growth rates may require more complex models if debiasing the computer model is of interest. Alternatively, given that the relative growth rate presented by (1) is well validated under a variety of other situations, it is possible that the measurement itself could be imperfect for example, if leaves were overlapping or if leaf thickness was not uniform throughout growth. By using the heteroscedastic modeling for the variance process and the orthogonal GP modeling for the discrepancy function, our approach provides reasonable prediction means and intervals for the experimental data, as well as discrepancy inference for computer modelers.

The estimated relative growth rates, $\hat{\theta}$, are reported in Table 1, where the confidence intervals are constructed based on the result of Theorem 3.1. First, we observe that

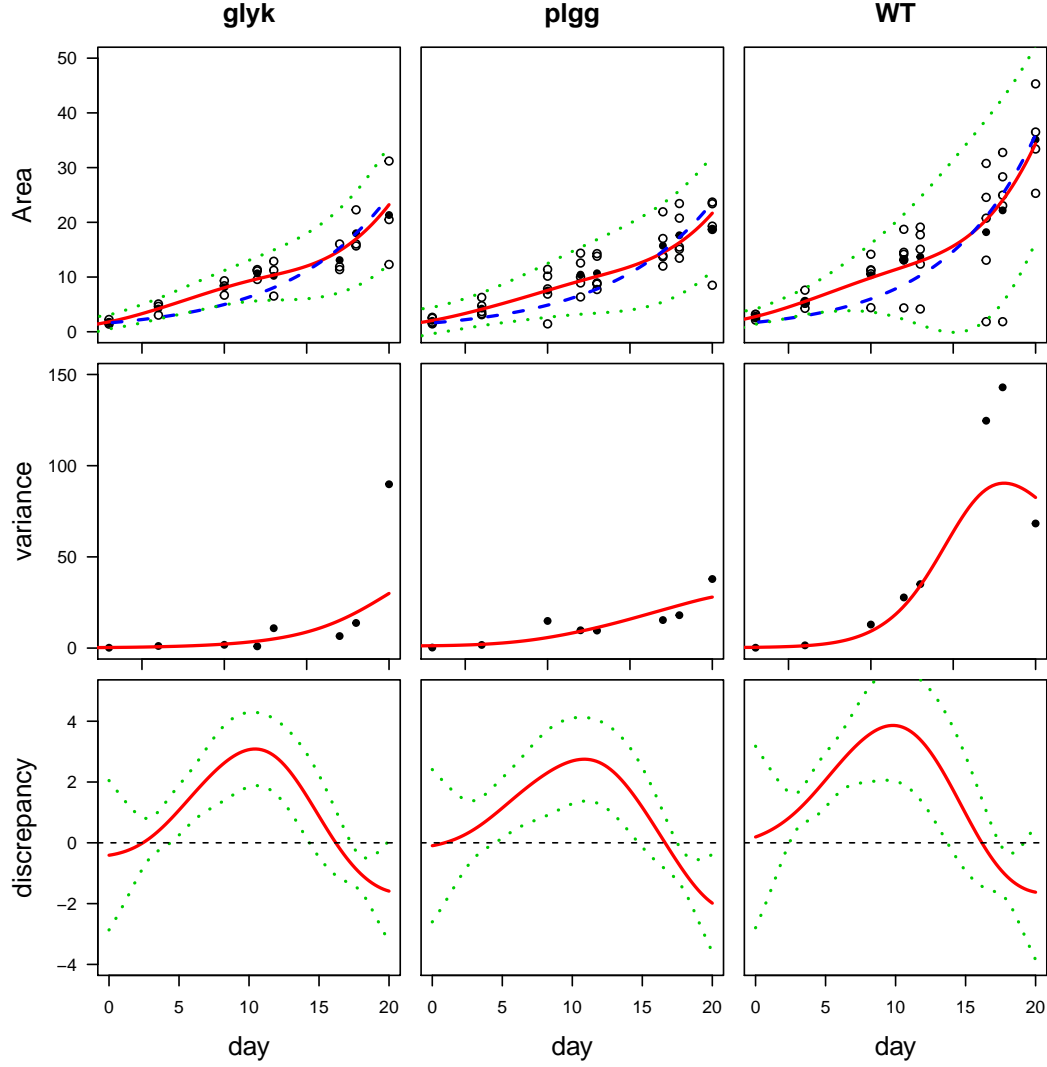


Figure 6: Calibration results of the three plant groups under ambient CO_2 : glyk (left), plgg (middle), and WY (right). Top panels represent the replicates as open circles with the averaged observation \hat{y}_i in filled circles at each input location, the curve $f(x, \hat{\theta})$ as a blue dashed line, and the prediction mean curve as a red solid line, with 95% prediction intervals in green dotted lines. Middle panels represent the sample variance $\hat{r}(\bar{x}_i)$ as black points, and the fitted variance process as a red solid line. Lower panels represent the mean curve of the discrepancy function, with 95% pointwise confidence intervals in green dotted lines.

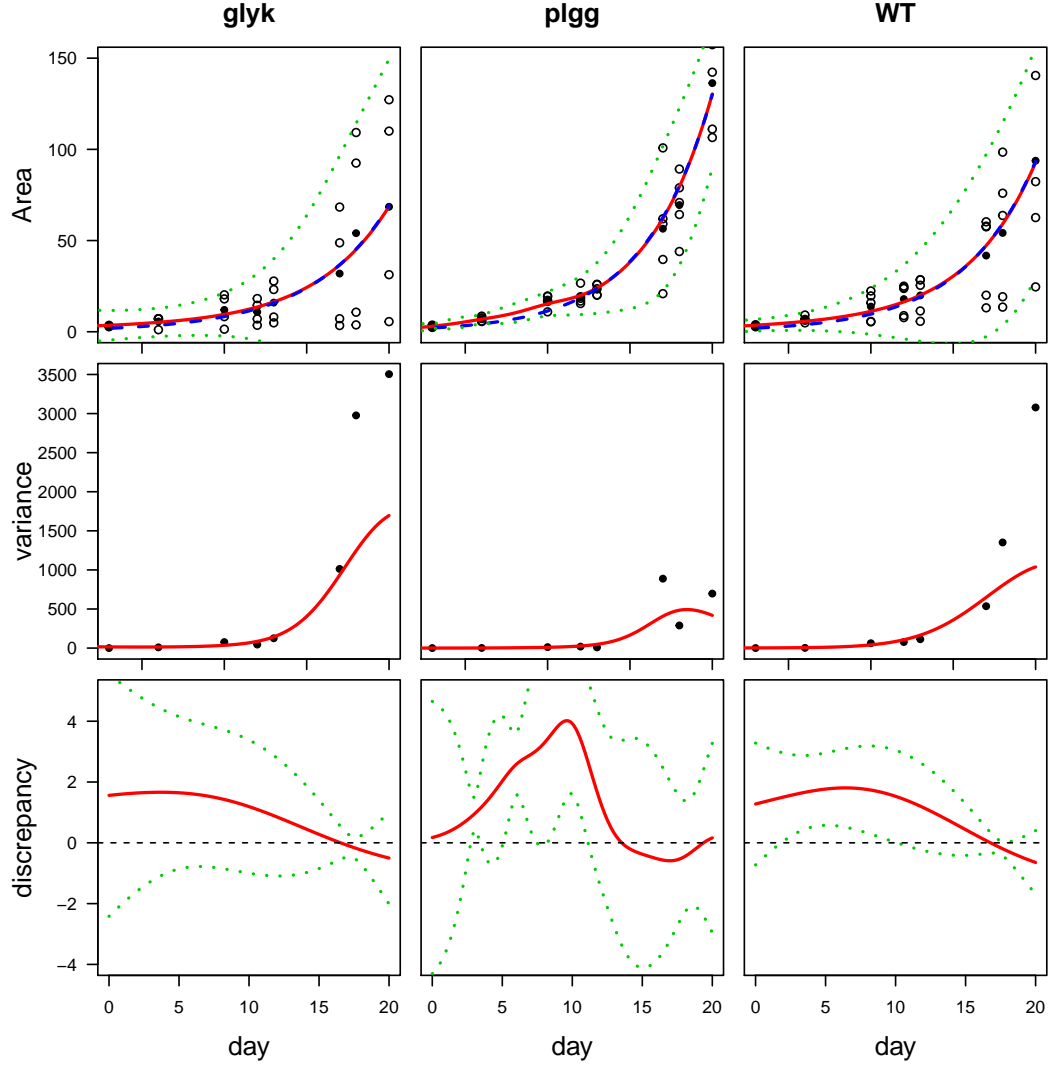


Figure 7: Calibration results of the three plant groups under high CO_2 : glyk (left), plgg (middle), and WY (right). Top panels represent the replicates as open circles with the averaged observation \hat{y}_i in filled circles at each input location, the curve $f(x, \hat{\theta})$ as a blue dashed line, and the prediction mean curve as a red solid line, with 95% prediction intervals in green dotted lines. Middle panels represent the sample variance $\hat{r}(\bar{x}_i)$ as black points, and the fitted variance process as a red solid line. Lower panels represent the mean curve of the discrepancy function, with 95% pointwise confidence intervals in green dotted lines.

relative growth rates under ambient CO₂ concentrations are slower than under high CO₂ concentrations across all plant groups. This is expected from the biological perspectives, because CO₂/O₂ under ambient CO₂ concentrations is low enough to drive high rates of photorespiration, which consumes energy and releases previously fixed carbon, decreasing growth. Secondly, as described in Section 2.1, the group *glyk* and *plgg* have slower relative growth rates than WT under ambient CO₂ concentrations, which is consistent with either a disruption in growth generally or specifically in photorespiration. Measurements under elevated CO₂ show that the growth rates of *glyk* and *plgg* increase with CO₂/O₂, providing evidence that the perturbations are directly related to photorespiration. Interestingly, rates of growth in *plgg* become statistically indistinguishable from WT under elevated CO₂, while the 95% confidence intervals of *glyk* and WT do not overlap, indicating that while elevated CO₂ is enough to rescue the growth phenotype of *plgg*, it is not sufficient to rescue *glyk*. Since rates of photorespiration should be effectively eliminated under elevated CO₂, this suggests that the gene GLYK may be important to other plant functions. These calibration parameter estimates provide insight into the values of the relative growth rates of different plant groups, which are difficult to determine by physical experiments due to the limitation of the existing experimental techniques.

To examine our approach, we compare the performance with Kennedy and O’Hagan’s approach and a traditional method in the biological literature (see, for example, Cousins et al. (2011)), which uses least-squares estimates for each individual replicate and then takes the average of them. That is, $\hat{\theta}_j = \arg \min_{\theta \in \Theta} \sum_{i=1}^n (y_i^{(j)} - f(\bar{x}_i, \theta))^2$ and obtain the estimate by $\hat{\theta} = \sum_{j=1}^a \hat{\theta}_j / a$, where a is the number of replicates. We use the experimental data under ambient CO₂ concentrations as an illustration, which is shown in Figure 8. Our approach appears to improve the calibration performance over the traditional method and Kennedy and O’Hagan’s approach, in the sense that the computer model outputs with our

CO ₂ Concentration	Group	Relative Growth Rate	
		Estimate	95% Confidence Interval
Ambient	<i>glyk</i>	0.1605	[0.1528, 0.1684]
	<i>plgg</i>	0.1582	[0.1513, 0.1651]
	WT	0.1792	[0.1704, 0.1880]
High	<i>glyk</i>	0.2119	[0.1928, 0.2310]
	<i>plgg</i>	0.2434	[0.2376, 0.2493]
	WT	0.2269	[0.2162, 0.2375]

Table 1: *Estimated relative growth rates.*

calibration parameter estimates, $f(x, \hat{\theta})$ in the blue dashed line, appear to be closer to the experimental data compared to the other two methods. In addition, it also shows that the prediction intervals of Kennedy and O’Hagan’s approach are larger than one would expect, which was also observed in the illustrative examples in Section 4. This issue is resolved when the proposed heteroscedastic model is used.

6 Summary and Concluding Remarks

Calibration of computer models plays a crucial role in many scientific fields where computer models are essential to predict the reality. The existing methods in the statistics literature, however, mainly focus on calibration with homoscedastic errors. Motivated by an experiment of plant relative growth rates, where the noise levels can vary dramatically across different input locations, we introduce a new calibration method to address the heteroscedasticity, where a latent variable process is used to model the error variance and an orthogonal Gaussian process is used to model the misspecification of a computer model. Our numerical studies demonstrate that when the errors are not homoscedastic, our proposed method not only successfully estimates calibration parameters accurately, but it also provides accurate

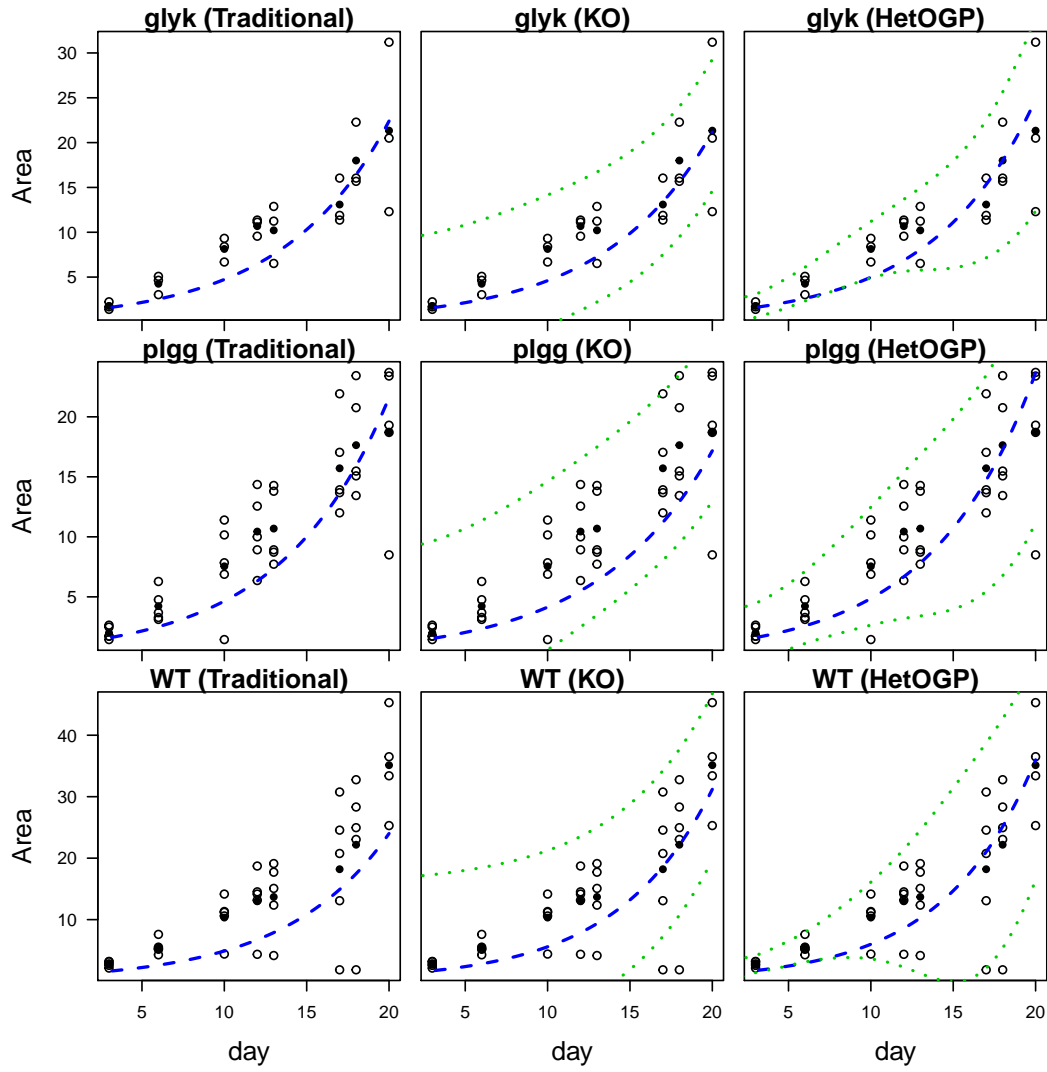


Figure 8: Comparison of the traditional method (left), Kennedy and O'Hagan's approach (middle), and the proposed method (right) based on the experimental data under ambient CO_2 , where the replicates are open circles with the averaged observation \bar{y}_i in filled circles, the curve $f(x, \hat{\theta})$ is the blue dashed line, and 95% prediction intervals are the green dotted lines. The three rows represent the three plant groups: *glyk* (top), *plgg* (middle), and WT (bottom).

predictions for a real system. The application to the plant relative growth rates illustrates that the proposed calibration method produces more statistically robust conclusions from computer models of biology and presumably biochemistry in general, and also provides more reasonable prediction and uncertainty quantification for the physical experiments.

This work lays the foundation for determining the optimal sampling time selection for the relative growth rates and other time-resolved heteroscedastic processes in biology and biochemistry. Since a physical experiment is often time consuming and limited by the number of plants that can be grown, an efficient sampling strategy becomes indispensable for conducting the experiment. To this end, we are working on an optimal sampling scheme for estimating time-resolved biological and biochemical measurements in plant biology, based upon the model and calibration procedure proposed herein. This will be of benefit not only to growth rate studies using simple computer models, but also more complex models such as those used to resolve fluxes through a plant metabolic network (Ma et al., 2014). Some existing techniques in the experimental design and active learning literature, such as A-optimal designs and sequential data selection by maximizing information entropy (MacKay, 1992; Cohn, 1994), can prove to be useful for conducting such a task.

This work also indicates several avenues for future research. First, instead of maximum likelihood estimation, Bayesian techniques can be naturally applied to the proposed method. Specifically, one could assign the priors of the calibration parameters as well as the hyperparameters in the model, and then draw samples from the posterior distribution using Markov chain Monte Carlo approaches, such as the Metropolis-Hastings sampler. Moreover, it is worth exploring other modeling techniques for the discrepancy function which also address the identifiability issue of the calibration parameters, such as Gu and Wang (2018), Tuo (2019), Xie and Xu (2018), and Dai and Chien (2018). These methods provide the potential to extend the proposed method with some theoretical guarantees.

Acknowledgements: We recognize funding by the Division of Chemical Sciences, Geosciences and Biosciences, Office of Basic Energy Sciences of the U.S. Department of Energy Grant DE-FG02-91ER20021 (B.W.).

References

- Ankenman, B., Nelson, B. L., and Staum, J. (2010). Stochastic kriging for simulation metamodeling. *Operations Research*, 58(2):371–382.
- Antoniewicz, M. R., Kelleher, J. K., and Stephanopoulos, G. (2006). Determination of confidence intervals of metabolic fluxes estimated from stable isotope measurements. *Metabolic Engineering*, 8(4):324–337.
- Bayarri, M., Berger, J., Cafeo, J., Garcia-Donato, G., Liu, F., Palomo, J., Parthasarathy, R., Paulo, R., Sacks, J., Walsh, D., et al. (2007a). Computer model validation with functional output. *The Annals of Statistics*, 35(5):1874–1906.
- Bayarri, M. J., Berger, J. O., Paulo, R., Sacks, J., Cafeo, J. A., Cavendish, J., Lin, C.-H., and Tu, J. (2007b). A framework for validation of computer models. *Technometrics*, 49(2):138–154.
- Binois, M. and Gramacy, R. B. (2019). *hetGP: Heteroskedastic Gaussian Process Modeling and Design under Replication*. R package version 1.1.1.
- Binois, M., Gramacy, R. B., and Ludkovski, M. (2018). Practical heteroscedastic Gaussian process modeling for large simulation experiments. *Journal of Computational and Graphical Statistics*, 27(4):808–821.
- Blackman, V. H. (1919). The compound interest law and plant growth. *Annals of Botany*, 33(131):353–360.
- Boldt, R., Edner, C., Kolukisaoglu, Ü., Hagemann, M., Weckwerth, W., Wienkoop, S., Morgenthal, K., and Bauwe, H. (2005). D-GLYCERATE 3-KINASE, the last unknown

- enzyme in the photorespiratory cycle in arabidopsis, belongs to a novel kinase family. *The Plant Cell*, 17(8):2413–2420.
- Byrd, R. H., Lu, P., Nocedal, J., and Zhu, C. (1995). A limited memory algorithm for bound constrained optimization. *SIAM Journal on Scientific Computing*, 16(5):1190–1208.
- Caffisch, R. E. (1998). Monte Carlo and quasi-Monte Carlo methods. *Acta Numerica*, 7(1):1–49.
- Cohn, D. A. (1994). Neural network exploration using optimal experiment design. In *Advances in Neural Information Processing Systems*, pages 679–686.
- Cousins, A. B., Walker, B. J., Pracharoenwattana, I., Smith, S. M., and Badger, M. R. (2011). Peroxisomal hydroxypyruvate reductase is not essential for photorespiration in arabidopsis but its absence causes an increase in the stoichiometry of photorespiratory co2 release. *Photosynthesis Research*, 108(2-3):91–100.
- Dai, X. and Chien, P. (2018). Another look at statistical calibration: a non-asymptotic theory and prediction-oriented optimality. *arXiv preprint arXiv:1802.00021*.
- Evans, J. R. and Poorter, H. (2001). Photosynthetic acclimation of plants to growth irradiance: the relative importance of specific leaf area and nitrogen partitioning in maximizing carbon gain. *Plant, Cell and Environment*, 24(8):755–767.
- Foyer, C. H., Bloom, A. J., Queval, G., and Noctor, G. (2009). Photorespiratory metabolism: genes, mutants, energetics, and redox signaling. *Annual Review of Plant Biology*, 60(1):455–484.
- Gneiting, T. and Raftery, A. E. (2007). Strictly proper scoring rules, prediction, and estimation. *Journal of the American Statistical Association*, 102(477):359–378.

- Goldberg, P. W., Williams, C. K., and Bishop, C. M. (1998). Regression with input-dependent noise: A Gaussian process treatment. In *Advances in Neural Information Processing Systems*, pages 493–499.
- Gramacy, R. B., Bingham, D., Holloway, J. P., Grosskopf, M. J., Kuran, C. C., Rutter, E., Tranter, M., and Drake, R. P. (2015). Calibrating a large computer experiment simulating radiative shock hydrodynamics. *The Annals of Applied Statistics*, 9(3):1141–1168.
- Gu, M. and Wang, L. (2018). Scaled Gaussian stochastic process for computer model calibration and prediction. *SIAM/ASA Journal on Uncertainty Quantification*, 6(4):1555–1583.
- Han, G., Santner, T. J., and Rawlinson, J. J. (2009). Simultaneous determination of tuning and calibration parameters for computer experiments. *Technometrics*, 51(4):464–474.
- Harville, D. A. (1998). *Matrix Algebra from a Statistician’s Perspective*. New York: Springer-Verlag.
- Higdon, D., Gattiker, J., Williams, B., and Rightley, M. (2008). Computer model calibration using high-dimensional output. *Journal of the American Statistical Association*, 103(482):570–583.
- Higdon, D., Kennedy, M., Cavendish, J. C., Cafo, J. A., and Ryne, R. D. (2004). Combining field data and computer simulations for calibration and prediction. *SIAM Journal on Scientific Computing*, 26(2):448–466.
- Hoffmann, W. A. and Poorter, H. (2002). Avoiding bias in calculations of relative growth rate. *Annals of Botany*, 90(1):37–42.

- Hunt, R. (1982a). Plant growth analysis: second derivatives and compounded second derivatives of splined plant growth curves. *Annals of Botany*, 50(3):317–328.
- Hunt, R. (1982b). *Plant Growth Curves. The Functional Approach to Plant Growth Analysis*. Edward Arnold Ltd.
- Kennedy, M. C. and O’Hagan, A. (2001). Bayesian calibration of computer models. *Journal of the Royal Statistical Society: Series B*, 63(3):425–464.
- Leister, D., Varotto, C., Pesaresi, P., Niwergall, A., and Salamini, F. (1999). Large-scale evaluation of plant growth in arabidopsis thaliana by non-invasive image analysis. *Plant Physiology and Biochemistry*, 37(9):671–678.
- Loeppky, J., Bingham, D., and Welch, W. (2006). Computer model calibration or tuning in practice. Technical report, University of British Columbia, Vancouver, BC, Canada.
- Ma, F., Jazmin, L. J., Young, J. D., and Allen, D. K. (2014). Isotopically nonstationary ^{13}C flux analysis of changes in arabidopsis thaliana leaf metabolism due to high light acclimation. *Proceedings of the National Academy of Sciences*, 111(47):16967–16972.
- MacKay, D. J. C. (1992). Information-based objective functions for active data selection. *Neural Computation*, 4(4):590–604.
- Mak, S., Sung, C.-L., Wang, X., Yeh, S.-T., Chang, Y.-H., Joseph, V. R., Yang, V., and Wu, C. F. J. (2018). An efficient surrogate model for emulation and physics extraction of large eddy simulations. *Journal of the American Statistical Association*, 113(524):1443–1456.
- Mardia, K. V. and Marshall, R. J. (1984). Maximum likelihood estimation of models for residual covariance in spatial regression. *Biometrika*, 71(1):135–146.

- Maurino, V. G. and Peterhansel, C. (2010). Photorespiration: current status and approaches for metabolic engineering. *Current Opinion in Plant Biology*, 13(3):248–255.
- Murchie, E. H. and Lawson, T. (2013). Chlorophyll fluorescence analysis: a guide to good practice and understanding some new applications. *Journal of Experimental Botany*, 64(13):3983–3998.
- Pick, T. R., Brutigam, A., Schulz, M. A., Obata, T., Fernie, A. R., and M. Weber, A. P. (2013). Plgg1, a plastidic glycolate glycerate transporter, is required for photorespiration and defines a unique class of metabolite transporters. *Proceedings of the National Academy of Sciences*, 110(8):3185–3190.
- Plumlee, M. (2017). Bayesian calibration of inexact computer models. *Journal of the American Statistical Association*, 112(519):1274–1285.
- R Core Team (2018). *R: A Language and Environment for Statistical Computing*. R Foundation for Statistical Computing, Vienna, Austria.
- Sacks, J., Welch, W. J., Mitchell, T. J., and Wynn, H. P. (1989). Design and analysis of computer experiments. *Statistical Science*, 4(4):409–423.
- Santner, T. J., Williams, B. J., and Notz, W. I. (2018). *The Design and Analysis of Computer Experiments (Second Edition)*. Springer New York.
- Schneider, C. A., Rasband, W. S., and Eliceiri, K. W. (2012). NIH image to ImageJ: 25 years of image analysis. *Nature Methods*, 9(7):671.
- Sharkey, T. D., Bernacchi, C. J., Farquhar, G. D., and Singsaas, E. L. (2007). Fitting photosynthetic carbon dioxide response curves for C_3 leaves. *Plant, Cell and Environment*, 30(9):1035–1040.

- Soetaert, K. (2009). *rootSolve: Nonlinear root finding, equilibrium and steady-state analysis of ordinary differential equations*. R package 1.6.
- South, P. F., Walker, B. J., Cavanagh, A. P., Rolland, V., Badger, M., and Ort, D. R. (2017). Bile acid sodium symporter bass6 can transport glycolate and is involved in photorespiratory metabolism in *Arabidopsis thaliana*. *The Plant Cell*, 29(4):808–823.
- Sung, C.-L., Hung, Y., Rittase, W., Zhu, C., and Wu, C. F. J. (2019). Calibration for computer experiments with binary responses and application to cell adhesion study. *Journal of the American Statistical Association*, accepted with minor revision.
- Sweeting, T. J. (1980). Uniform asymptotic normality of the maximum likelihood estimator. *The Annals of Statistics*, 8(6):1375–1381.
- Tuo, R. (2019). Adjustments to computer models via projected kernel calibration. *SIAM/ASA Journal on Uncertainty Quantification*, 7(2):553–578.
- Tuo, R. and Wu, C. F. J. (2015). Efficient calibration for imperfect computer models. *The Annals of Statistics*, 43(6):2331–2352.
- Tuo, R. and Wu, C. F. J. (2016). A theoretical framework for calibration in computer models: parametrization, estimation and convergence properties. *SIAM/ASA Journal on Uncertainty Quantification*, 4(1):767–795.
- von Caemmerer, S. (2000). *Biochemical Models of Leaf Photosynthesis*. CSIRO Publishing.
- von Caemmerer, S. (2013). Steady-state models of photosynthesis. *Plant, Cell and Environment*, 36(9):1617–1630.

- Walker, B. J., South, P. F., and Ort, D. R. (2016a). Physiological evidence for plasticity in glycolate/glycerate transport during photorespiration. *Photosynthesis research*, 129(1):93–103.
- Walker, B. J., VanLoocke, A., Bernacchi, C. J., and Ort, D. R. (2016b). The costs of photorespiration to food production now and in the future. *Annual Review of Plant Biology*, 67(1):107–129.
- Wang, S., Chen, W., and Tsui, K.-L. (2009). Bayesian validation of computer models. *Technometrics*, 51(4):439–451.
- Wang, W. and Haaland, B. (2019). Controlling sources of inaccuracy in stochastic kriging. *Technometrics*, 61(3):309–321.
- Wang, X., Wang, Y., and Yang, V. (2018). Three-dimensional study of gas-centered, liquid-swirl coaxial injector flow dynamics at supercritical condition. *Bulletin of the American Physical Society*.
- Wong, R. K. W., Storlie, C. B., and Lee, T. C. M. (2017). A frequentist approach to computer model calibration. *Journal of the Royal Statistical Society: Series B*, 79(2):635–648.
- Xie, F. and Xu, Y. (2018). Bayesian projected calibration of computer models. *arXiv preprint arXiv:1803.01231*.
- Xu, L., Cruz, J. A., Savage, L. J., Kramer, D. M., and Chen, J. (2015). Plant photosynthesis phenomics data quality control. *Bioinformatics*, 31(11):1796–1804.
- Yeh, S.-T., Wang, X., Sung, C.-L., Mak, S., Chang, Y.-H., Zhang, L., Wu, C. J., and Yang, V. (2018). Common proper orthogonal decomposition-based spatiotemporal emulator for design exploration. *AIAA Journal*, 56(6):2429–2442.

Supplementary Materials for “Calibration of Computer Models with Heteroscedastic Errors and Application to Plant Relative Growth Rates”

S1 Gradient of (8)

In this section, we derive the gradient of the log-likelihood of (8), which can be used for a Newton-like optimization method.

First, we use the Woodbury identity (Harville, 1998) to simplify the log-likelihood. By (9) and (10), we have

$$\begin{aligned}\hat{\nu} = & \frac{1}{N} (\mathbf{Y}_N - \mathbf{f}(\theta))^T \mathbf{\Lambda}_N^{-1} (\mathbf{Y}_N - \mathbf{f}(\theta)) - \frac{1}{N} (\bar{\mathbf{Y}}_n - \bar{\mathbf{f}}(\theta))^T \mathbf{A}_n \mathbf{\Lambda}_n^{-1} (\bar{\mathbf{Y}}_n - \bar{\mathbf{f}}(\theta)) \\ & + \frac{1}{N} (\bar{\mathbf{Y}}_n - \bar{\mathbf{f}}(\theta))^T (\mathbf{K}_n + \mathbf{A}_n^{-1} \mathbf{\Lambda}_n)^{-1} (\bar{\mathbf{Y}}_n - \bar{\mathbf{f}}(\theta))\end{aligned}$$

and

$$\begin{aligned}\log L = & -\frac{N}{2} \log \hat{\nu} - \frac{1}{2} \log |\mathbf{K}_n + \mathbf{A}_n^{-1} \mathbf{\Lambda}_n| - \frac{1}{2} \sum_{i=1}^n [(a_i - 1) \log \lambda_i + \log a_i] \\ & - \frac{n}{2} \log \hat{\nu}_{(g)} - \frac{1}{2} \log |\mathbf{K}_{(g)} + g \mathbf{A}_n^{-1}| + \text{Constant}.\end{aligned}$$

Define $\mathbf{\Gamma}_n = \mathbf{K}_n + \mathbf{A}_n^{-1} \mathbf{\Lambda}_n$ and $\mathbf{\Gamma}_{(g)} = \mathbf{K}_{(g)} + g \mathbf{A}_n^{-1}$. For each component φ_j of the lengthscale in the kernel function k , we have

$$\frac{\partial \log L}{\partial \varphi_j} = \frac{1}{2\hat{\nu}} (\bar{\mathbf{Y}}_n - \bar{\mathbf{f}}(\theta))^T \mathbf{\Gamma}_n^{-1} \frac{\partial \mathbf{K}_n}{\partial \varphi_j} \mathbf{\Gamma}_n^{-1} (\bar{\mathbf{Y}}_n - \bar{\mathbf{f}}(\theta)) - \frac{1}{2} \text{tr} \left(\mathbf{\Gamma}_n^{-1} \frac{\partial \mathbf{K}_n}{\partial \varphi_j} \right).$$

Here we use Monte Carlo integration (Caffisch, 1998) to approximate the orthogonal kernel matrix \mathbf{K}_n . Suppose that the samples ξ_1, \dots, ξ_m are uniformly drawn from χ ,

and denote that $w(x) = (k_0(x, \xi_1), \dots, k_0(x, \xi_m))^T \in \mathbb{R}^{m \times 1}$, $\mathbf{w} = (w(\bar{x}_1), \dots, w(\bar{x}_n)) \in \mathbb{R}^{m \times n}$, $\mathbf{F}_\theta = (\frac{\partial f(\xi_1, \theta)}{\partial \theta^T}, \dots, \frac{\partial f(\xi_m, \theta)}{\partial \theta^T})^T \in \mathbb{R}^{m \times q}$, $\mathbf{W} = (k_0(\xi_i, \xi_j))_{1 \leq i, j \leq m} \in \mathbb{R}^{m \times m}$, and $\mathbf{K}_0 = (k_0(\bar{x}_i, \bar{x}_j))_{1 \leq i, j \leq n} \in \mathbb{R}^{n \times n}$. Then, by following (7) and approximating the integration by the Monte Carlo samples, we have

$$\mathbf{K}_n = \mathbf{K}_0 - \mathbf{w}^T \mathbf{F}_\theta (\mathbf{F}_\theta^T \mathbf{W} \mathbf{F}_\theta)^{-1} \mathbf{F}_\theta^T \mathbf{w}.$$

Thus, we have

$$\begin{aligned} \frac{\partial \mathbf{K}_n}{\partial \varphi_j} &= \frac{\partial \mathbf{K}_0}{\partial \varphi_j} - 2 \frac{\partial \mathbf{w}^T}{\partial \varphi_j} \mathbf{F}_\theta (\mathbf{F}_\theta^T \mathbf{W} \mathbf{F}_\theta)^{-1} \mathbf{F}_\theta \mathbf{w} \\ &\quad + \mathbf{w}^T \mathbf{F}_\theta (\mathbf{F}_\theta^T \mathbf{W} \mathbf{F}_\theta)^{-1} \left(\mathbf{F}_\theta^T \frac{\partial \mathbf{W}}{\partial \varphi_j} \mathbf{F}_\theta \right) (\mathbf{F}_\theta^T \mathbf{W} \mathbf{F}_\theta)^{-1} \mathbf{F}_\theta \mathbf{w}. \end{aligned}$$

For common choices of kernels for k_0 , such as Gaussian or Matérn kernels, the derivative, $\partial \mathbf{K}_0 / \partial \varphi_j$, can be expressed in a closed form.

For the latent variance parameters, δ_i , in Δ_n , we have

$$\frac{\partial \log L}{\partial \Delta_n} = \frac{\partial \Lambda_n}{\partial \Delta_n} \frac{\partial \log L}{\partial \Lambda_n} - \frac{\Gamma_{(g)}^{-1} \Delta_n}{\hat{\nu}_{(g)}} = \Lambda_n \mathbf{K}_{(g)} \Gamma_{(g)}^{-1} \frac{\partial \log L}{\partial \Lambda_n} - \frac{\Gamma_{(g)}^{-1} \Delta_n}{\hat{\nu}_{(g)}},$$

where

$$\frac{\partial \log L}{\partial \Lambda_n} = \frac{1}{2} \frac{\mathbf{A}_n \mathbf{S} \Lambda_n^{-2} + \mathbf{A}_n^{-1} \text{diag}(\Gamma_n^{-1} \bar{\mathbf{Y}}_n)^2}{\hat{\nu}} - \frac{\mathbf{A}_n - \mathbf{I}_n}{2} \Lambda_n^{-1} - \frac{1}{2} \mathbf{A}_n^{-1} \text{diag}(\Gamma_n^{-1}),$$

where $\mathbf{S} = \text{diag}(s_1^2, \dots, s_n^2)$ and $s_i = \sum_{j=1}^{a_i} (y_i^{(j)} - \bar{y}_i)^2 / a_i$.

For the each component ϕ_j of the lengthscale ϕ in the kernel function $k_{(g)}$ of the noise

process, we have

$$\begin{aligned} \frac{\partial \log L}{\partial \phi_j} &= \left[\frac{\partial \mathbf{K}_{(g)}}{\partial \phi_j} - \mathbf{K}_{(g)} \mathbf{\Gamma}_{(g)}^{-1} \frac{\partial \mathbf{K}_{(g)}}{\partial \phi_j} \right] \mathbf{\Gamma}_{(g)}^{-1} \mathbf{\Delta}_n \mathbf{\Lambda}_n \times \frac{\partial \log L}{\partial \mathbf{\Lambda}_n} \\ &\quad + \frac{1}{2\hat{\nu}_{(g)}} \mathbf{\Delta}_n^T \mathbf{\Gamma}_{(g)}^{-1} \frac{\partial \mathbf{K}_{(g)}}{\partial \phi_j} \mathbf{\Gamma}_{(g)}^{-1} \mathbf{\Delta}_n - \text{tr} \left(\mathbf{\Gamma}_{(g)}^{-1} \frac{\partial \mathbf{K}_{(g)}}{\partial \phi_j} \right). \end{aligned}$$

Similarly, for common choices of kernels for $k_{(g)}$, such as Gaussian or Matérn kernels, the derivative, $\partial \mathbf{K}_{(g)} / \partial \phi_j$, has a closed form.

For the nugget parameter g , we have

$$\frac{\partial \log L}{\partial g} = -\mathbf{K}_{(g)} \mathbf{\Gamma}_{(g)}^{-1} \mathbf{A}_n^{-1} \mathbf{\Gamma}_{(g)}^{-1} \mathbf{\Delta}_n \mathbf{\Lambda}_n \times \frac{\partial \log L}{\partial \mathbf{\Lambda}_n} + \frac{1}{2\hat{\nu}_{(g)}} \mathbf{\Delta}_n^T \mathbf{\Gamma}_{(g)}^{-1} \mathbf{A}_n^{-1} \mathbf{\Gamma}_{(g)}^{-1} \mathbf{\Delta}_n - \text{tr} \left(\mathbf{A}_n^{-1} \mathbf{\Gamma}_{(g)}^{-1} \right)$$

Finally, for each component θ_j of the calibration parameter θ ,

$$\frac{\partial \log L}{\partial \theta_j} = -\frac{1}{2\hat{\nu}} \frac{\partial N\hat{\nu}}{\partial \theta_j} - \frac{1}{2} \text{tr} \left(\mathbf{\Gamma}_n^{-1} \frac{\partial \mathbf{K}_n}{\partial \theta_j} \right),$$

where

$$\begin{aligned} \frac{\partial N\hat{\nu}}{\partial \theta_j} &= -2\mathbf{\Lambda}_N^{-1} (\mathbf{Y}_N - \mathbf{f}(\theta))^T \frac{\partial \mathbf{f}(\theta)}{\partial \theta_j} + 2\mathbf{A}_n \mathbf{\Lambda}_n^{-1} (\bar{\mathbf{Y}}_n - \bar{\mathbf{f}}(\theta))^T \frac{\partial \bar{\mathbf{f}}(\theta)}{\partial \theta_j} \\ &\quad - 2\mathbf{\Gamma}_n^{-1} (\bar{\mathbf{Y}}_n - \bar{\mathbf{f}}(\theta))^T \frac{\partial \bar{\mathbf{f}}(\theta)}{\partial \theta_j} - (\bar{\mathbf{Y}}_n - \bar{\mathbf{f}}(\theta))^T \mathbf{\Gamma}_n^{-1} \frac{\partial \mathbf{K}_n}{\partial \theta_j} \mathbf{\Gamma}_n^{-1} (\bar{\mathbf{Y}}_n - \bar{\mathbf{f}}(\theta)), \end{aligned}$$

and

$$\frac{\partial \mathbf{K}_n}{\partial \theta_j} = -2\mathbf{w}^T \frac{\partial \mathbf{F}}{\partial \theta_j} (\mathbf{F}^T \mathbf{W} \mathbf{F})^{-1} \mathbf{F} \mathbf{w} + 2\mathbf{w}^T \mathbf{F} (\mathbf{F}^T \mathbf{W} \mathbf{F})^{-1} \left(\frac{\partial \mathbf{F}^T}{\partial \theta_j} \mathbf{W} \mathbf{F} \right) (\mathbf{F}^T \mathbf{W} \mathbf{F})^{-1} \mathbf{F} \mathbf{w}.$$

S2 Regularity Conditions of Theorem 3.1

The regularity conditions for Theorem 3.1 are given below.

1. The kernels k and $k_{(g)}$ are twice differentiable on the parameter spaces of $\theta, \boldsymbol{\varphi}$ and $\boldsymbol{\phi}$ with continuous second derivatives.
2. The smallest latent root of \mathbf{B}_N tends to ∞ as $N \rightarrow \infty$.
3. $\mathbf{B}_N^{-1/2} \left(\frac{\partial^2 \log L}{\partial \boldsymbol{\omega} \partial \boldsymbol{\omega}^T} \right) \mathbf{B}_N^{-1/2}$ converges in probability to a unit matrix.

References

Harville, D. A. (1998). *Matrix Algebra from a Statisticians Perspective*. Springer, New York.